Materials Advances

ROYAL SOCIETY OF CHEMISTRY

PAPER

View Article Online
View Journal | View Issue

Cite this: *Mater. Adv.*, 2026, 7, 3708

Energy transfer from Ag species to Nd^{3+} in Ga–fluoride–phosphate glasses: near-infrared emission enhancement *via* controlled heat treatment and femtosecond laser inscription

Vinicius D. Jesus, *[a] Leonnam G. Merizio, [ab] Gustavo Galleani,[a] Guillaume Raffy, [c] Mathis Carpentier,[d] Yannick Petit, *[d] Thierry Cardinal[d] and Andrea S. S. de Camargo *[ef]

Gallium fluoride–phosphate glasses are promising materials with wide optical transmission window, high volumetric density, and the ability to accommodate high concentrations of rare earth dopant ions within a tailored fluoride-rich coordination environment, resulting in high emission cross sections. In this work, the compositional system $25Ga(PO_3)_3$–$20ZnF_2$–$30BaF_2$–$(25–x–y)SrF_2$–$xAgNO_3$–$yNdF_3$ (x = 0–10 mol%, y = 0 or 1 mol%) was studied to understand how silver species affect the near-infrared (NIR) emission of Nd^{3+} ions, when the glasses are subjected to controlled heat treatment and to femtosecond direct laser writing (DLW). The glasses were obtained *via* the melt-quenching technique and characterized by DSC, XRD, UV-Vis-NIR absorption, and PL spectroscopy. The as-prepared glasses show broad UV-Vis excitation and emission bands arising from the coexistence of Ag^+ ions and ionic Ag pairs. In samples with 10 mol% Ag^+, brownish coloration and modified emission profiles indicated Ag nanoparticle formation at the surface. Heat treatment promoted the conversion of isolated Ag^+ into ionic pairs, producing broadband emissions tunable by excitation wavelength and Ag^+ concentration. In co-doped samples, Nd^{3+} introduced absorption dips in the Ag-related UV-Vis bands, consistent with energy transfer, which was further confirmed by shortened Ag excited-state lifetimes and increased Nd^{3+} NIR emission under UV-Vis excitation. In order to control the spatial distribution and size of Ag aggregates (nanoclusters, NCs) and to increase the energy transfer efficiency to Nd^{3+}, femtosecond direct laser writing (DLW) was employed to co-doped glasses with 3 and 5 mol% Ag^+. This approach enabled three-dimensional localized growth of Ag NCs with sub-micron spatial control. In the laser processed regions, the NIR emissions of Nd^{3+} at 900 and 1060 nm were significantly enhanced, clearly evidencing enhanced energy transfer from the localized laser-induced Ag-NCs to the Nd^{3+} ions. These findings suggest the possibility of tailoring high optical contrast near-IR emissions in glasses, enabling progress in advanced photonic applications.

Received 8th December 2025,
Accepted 2nd March 2026

DOI: 10.1039/d5ma01430a

rsc.li/materials-advances

1. Introduction

Efficient trivalent rare-earth (RE^{3+}) based glass systems for photonic device applications demand hosts that combine high dopant ion solubility, suitable phonon energy, and broad optical transparency. Fluoride-phosphate (FP) glasses are promising candidates that offer the possibility of tailored properties by proper choice of composition.[1,2] They present a wide optical transparence window (180–4000 nm), a fairly low melting temperature (~900 °C), and can accommodate relatively high RE^{3+} concentrations, enabling applications as optical fibers, amplifiers and solid-state lasers.[3,4] To that end, Nd^{3+} is one of the most explored ions with near-IR emissions of interest at 1060 and 1340 nm, corresponding to the $^4F_{3/2} \rightarrow {}^4I_{11/2}$, and $^4F_{3/2} \rightarrow {}^4I_{13/2}$ transitions, respectively.[5]

Despite their well-known technological importance, the intra-configurational f–f transitions of RE^{3+} ions are electric dipole forbidden yielding low absorption and emission cross sections. Besides, the shielding of the internal 4f orbitals from

[a] São Carlos Institute of Physics, University of São Paulo, São Carlos, SP, 13566-590, Brazil. E-mail: vinicius.duarte.jesus@usp.br
[b] São Carlos Institute of Chemistry, University of São Paulo, São Carlos, SP, 13566-590, Brazil
[c] Université de Bordeaux, CNRS, ISM, UMR 5255, F-33400 Talence, France
[d] Université de Bordeaux, CNRS, Bordeaux INP, ICMCB, UMR 5026, F-33600 Pessac, France. E-mail: yannick.petit@u-bordeaux.fr
[e] Federal Institute for Materials Research and Testing (BAM), Berlin, 12489, Germany. E-mail: andrea.camargo@bam.de
[f] Otto-Schott Institute of Materials Research, Friedrich-Schiller University, Jena, 07743, Germany

the ligand field in the vicinity of the ion, due to more external 5s and 5p orbitals, leads to transitions rather insensitive to the chemical environment. To increase emission efficiency, different strategies are sought, such as co-doping with sensitizer ions exhibiting higher absorption cross sections in convenient excitation ranges. A well-established example is Yb^{3+} presenting high absorption cross section at 980 nm – a wavelength where high intensity low cost diode lasers are commercially available, allowing the sensitization of Er^{3+} and Tm^{3+} ions.[6] Furthermore, co-doping with transition-metal ions has emerged as an alternative and versatile strategy to enhance RE^{3+} luminescence. Ions such as Ag^{+}, Cu^{+}, Au^{+}, and Pd^{2+} can introduce additional absorption channels and promote energy transfer processes or local-field enhancement effects, leading to improved RE^{3+} emission efficiencies in oxide, oxyfluoride, and fluoride glass hosts.[7–10]

The rich chemistry of Ag species has been explored particularly in silver-doped phosphate and fluorophosphate glasses. Depending on composition, concentration, and thermal history, silver can be stabilized as isolated ions, ion pairs, nanoclusters (NCs), or metallic nanoparticles (NPs), each contributing differently to the optical response of the material.[8] Ionic and cluster-like Ag species typically act as broadband sensitizers capable of transferring excitation energy to RE^{3+} ions, whereas metallic NPs can induce surface plasmon resonance (SPR), enhancing local electromagnetic fields and modifying RE^{3+} radiative decay rates.[11–18] Indirect enhancement of Nd^{3+} near-infrared emission has been demonstrated *via* $Ag^{+} \rightarrow Nd^{3+}$ energy transfer in phosphate-based glasses.[19] However, while these studies clearly establish the feasibility of transition-metal mediated enhancement of Nd^{3+} luminescence, they predominantly rely on global thermal treatments to control the formation and evolution of metal-related species. Such approaches intrinsically lack spatial selectivity, limiting the ability to locally tailor Ag–RE interaction sites within the glass volume for integrated elements such as laser-active photonic integrated circuits or highly-localized display devices.

An alternative and increasingly powerful route to overcome this limitation is the use of ultrafast laser irradiation. Direct laser writing (DLW) enables highly localized nonlinear absorption at the laser–matter interaction voxel, allowing precise spatial patterning of refractive index (Δn) and fluorescence contrast with sub-micrometric precision.[20] DLW has proven to be effective in enhancing Ag ion mobility and localized clustering, resulting in tailored luminescent or plasmonic regions that add functionality and improve the performance of both undoped and RE co-doped Ag-containing glasses.[7,16,21] Such laser-induced modifications has enabled the fabrication of integrated photonic elements, including waveguides and micro-optical devices, as well as laser-written structures exhibiting enhanced Yb^{3+} NIR emission mediated by Ag nanoclusters.[22] Recently, studies have been reported on bismuth-doped glasses, further demonstrating the versatility of laser-induced material modifications to promote locally energy transfer processes.[23] Although DLW has been explored in fluoride-phosphate glasses doped with silver,[9] there are no reports on Nd^{3+} doped FP glasses. The mixed-anion character in these glasses is particularly favorable for the solubility, mobility, and stabilization of Ag and RE species, while maintaining suitable phonon energy and mechanical robustness. There lies the motivation for this work to apply DLW to a novel fluoride phosphate glass, co-doped with silver and Nd^{3+}, and to study the effect of induced Ag species on Nd^{3+} near-infrared emission, in comparison to the heat treatment approach.

The choice for the gallium fluoride phosphate glass composition $Ga(PO_3)_3$–ZnF_2–BaF_2–SrF_2 investigated in this work derives from previous studies in our group in which we demonstrated very good glass homogeneity, high rare-earth ion solubility, and a broad optical transparency window of these glasses.[2] Structural investigations *via* solid-state NMR and EPR spectroscopies demonstrated that the RE ions are majorly coordinated by fluorine atoms which provides a low phonon energy local environment particularly favoring near-infrared emissions. Therefore, the composition serves as relevant platform to evaluate both the formation of Ag-related centers and the feasibility of laser-induced functional modifications aimed at photonic applications. Accordingly, the work presents the synthesis and comprehensive structural, thermal, and optical characterization of samples doped with varying Ag^{+} concentrations (1, 3, 5, and 10 mol%), and samples co-doped with 1 mol% Nd^{3+}. A comparative analysis between thermally treated bulk samples and laser-inscribed regions is performed to elucidate how different Ag species influence Nd^{3+} emission intensity and excited state lifetime values. By combining compositional control with spatially selective fs-laser processing, this study offers a demonstration of how Ag-related centers can be tailored to transfer energy to RE ions, thereby augmenting their emission intensities, which is relevant for functional applications.

2. Experimental

2.1 Preparation of glass samples

The glasses were prepared based on analogous compositions previously studied in our laboratory, containing $In(PO_3)_3$ and (ZnF_2, BaF_2, SrF_2) and doped with Eu^{3+}, Er^{3+}, and Yb^{3+} ions.[1,2,24,25] Based on the findings of structure–property correlations in them, this work focused on the preparation of the new molar composition $25Ga(PO_3)_3$–$20ZnF_2$–$30BaF_2$–$(25-y-x)$-SrF_2–$xAgNO_3$–$yNdF_3$, where x = 0, 1, 3, 5, and 10 mol%, and y = 0 and 1 mol%. The doping concentrations of Ag^{+} and Nd^{3+} were chosen based on initial tests to secure optical quality and to avoid devitrification, as listed in Table 1. The high-purity reagents ZnF_2 (99%, Sigma-Aldrich), BaF_2 (99%, Alfa Aesar), SrF_2 (99%, Alfa Aesar), $AgNO_3$ (99%, Sigma-Aldrich), NdF_3 (99.9%, Sigma-Aldrich), and Ga_2O_3 (99%, AmBeed) were used as purchased, while $Ga(PO_3)_3$ was obtained through a cryochemical reaction of phosphoric acid, in its crystalline form, mixed with gallium oxide in liquid nitrogen. The mixture was homogenized and then kept in a refrigerator ($\sim$5 °C) for 24 hours, followed by drying at 180 °C for 12 hours, and

Table 1 Molar fraction of Ag-doped and Ag/Nd co-doped glasses

Sample	$Ga(PO_3)_3$ (%)	ZnF_2 (%)	BaF_2 (%)	SrF_2 (%)	$AgNO_3$ (%)	NdF_3 (%)
Ga0Ag	25	20	30	25	0	0
Ga1Ag	25	20	30	24	1	0
Ga3Ag	25	20	30	22	3	0
Ga5Ag	25	20	30	20	5	0
Ga10Ag	25	20	30	15	10	0
Ga0Ag1Nd	25	20	30	24	0	1
Ga3Ag1Nd	25	20	30	21	3	1
Ga5Ag1Nd	25	20	30	19	5	1
Ga10Ag1Nd	25	20	30	14	10	1

subsequently treated at 300 °C, 600 °C, and 900 °C, remaining 30 minutes at each stage. The resulting phosphate was duly characterized before its use in glass preparation.[26]

The precursor powders were weighed on a semi-analytical balance, grinded, and homogenized in an agate mortar. The mixture was placed in a Pt crucible and subjected to melting at 900 °C, followed by thermal quench by placing the bottom of the crucible in water.[21,27] Due to the presence of silver in the composition, the annealing process was carried out at 50 °C below the glass transition temperature (T_g) for 4h in order to reduce internal stress in the glass network induced by the thermal shock, and to avoid cracking. The Ag-doped glasses were characterized before and after annealing to evaluate the heat treatment effect. Finally, the glasses were optically polished using sandpaper with grit sizes of 400, 600, 800, and 1200, and a diamond paste with 0.3 μm grains, to reach optical quality prior to spectroscopic characterization and direct laser writing experiments.

2.2 Thermal and spectroscopic characterization

The glass samples were thermally analyzed by Differential Scanning Calorimetry (DSC) on a NETZSCH STA 449F3, to determine the characteristic temperatures of glass transition (T_g), crystallization onset (T_x), and crystallization peak (T_p). The analyses were performed using monolithic samples with approximately 30–40 mg, at a heating rate of 10 °C min^{-1} up to 820 °C, in air atmosphere, with a flow rate of 60 mL min^{-1}.

Transmission spectra were measured in the range 250–1500 nm in a PerkinElmer UV-Vis spectrometer model Lambda 1050. At long wavelengths, transmission is limited by multi-phonon absorption, while the transparency limit at short wavelengths is imposed by electronic transitions of dopants. The photophysics of pristine samples, not subjected to laser structuring, were evaluated by steady state and time resolved (μs) photoluminescence (PL) in a Horiba Jobin Yvon Fluorolog 3 spectrofluorimeter. The excitation and emission spectra were collected in the UV-Vis-NIR range using a 450 W Xe lamp in CW and pulsed modes, as excitation source, and detectors included a PPD-850 photodiode (UV-Vis), a Hamamatsu H10331A-75 photomultiplier (NIR), and a Charge-Coupled Device (CCD) model Symphony II 356291 (NIR). Excited state lifetime values were obtained by fitting corresponding emission decay curves.

2.3 Direct laser writing and fluorescence lifetime imaging

The selected glass samples were irradiated by a Yb:KGW fs laser oscillator at 1030 nm (Amplitude system, up to 2.6 W average power, 9.8 MHz repetition rate, 390 fs pulse duration (FWHM)). The laser irradiance was controlled with an acousto-optic modulator enabling to cumulate laser pulses (up to $N = 10^5$–10^6 here) with energy ranging from 20 to 150 nJ. During writing, the sample positioning and displacement were carried out using a high-precision 3D translation stage (XMS-50 stages, Microcontroller). The laser beam was focused by a microscope objective (Carl Zeiss, 20× – 0.75NA) and all the structures were written 150 μm below the surface of the samples. The luminescent response of the DLW structures was characterized using a high spectral resolution micro-spectrometer (Lab-RAM HR800 from Horiba Jobin Yvon GmbH, Haching, Germany), with a 150 grooves cm^{-1} grating. The visible and NIR spectra were excited by a 405 nm laser diode (100 mW, TEM00, OBIS from COHERENT, Santa Clara, CA, USA) focalized with an Olympus objective (50×, NA 0.9).

The structures formed by DLW were successfully visualized and resolved with an Olympus FLUOVIEW FV1200 wide-field microscope using different objectives (10× – 0.30NA, 20× – 0.50NA, 60× – 0.75NA and 100× – 0.80NA). The images were acquired under both white light illumination and 365 nm excitation, allowing the observation of morphological details and the luminescent response of the modified regions.

Fluorescence lifetime imaging microscopy (FLIM) analysis were carried using a Picoquant MT200 microscope equipped with two MPD single photon avalanche diodes (SPADs) and a PicoHarp300 timing board for time-correlated single photon counting (TCSPC) operation. A pulsed laser at 405 nm (6 ps pulse duration, 4.75 MHz repetition rate, frequency-doubled Ti:Saphire mode-locked laser (MIRA, Coherent) tuned at 810 nm) was peaked on-demand by an acousto-optic pulse picker, then coupled to a 4 μm core polarization-maintaining fiber optic, and finally out-coupled with a clean Gaussian beam profile as to ensure optimal focusing by the microscope objective to achieve diffraction-limited excitation of the samples. A 100×, 1.40NA oil objective (UPLSAPO100XO, Olympus, Tokyo, Japan) was used for both excitation and collection of the fluorescence. A spectrally flat 80%T/20%R beam-splitter reflected the excitation beam to the objective and transmitted the fluorescence to a band-pass filter (with spectral transmission window of 470–550 nm) before the confocal optics and detectors. The laser was scanned using a piezoelectric stage in a grid pattern of 136 nm steps and typically 1–2 ms per pixel. For the calculation of FLIM images, ''FAST-FLIM'' algorithm was used, and lifetime distribution was calculated using the method reported by Petit *et al.*,[7] in which, for each pixel, the reported lifetime was calculated as the first statistical moment of the histogram of single photon arrival times, minus a reference time taken at the beginning of the decay curve. FLIM images include temporal and intensity information of the collected fluorescence, where the color code and the brightness levels represent the average FAST-FLIM arrival times and the number of collected events, respectively.

3. Results and discussions

3.1 Visual inspection and thermal properties

The samples doped with Ag^{+} and co-doped with Nd^{3+} were all obtained with high optical quality and no sign of devitrification (Fig. 1). The silver doped samples remained colorless up to 5 mol% Ag^{+}, while 10 mol% doping led to a brownish coloration (Fig. 1a), suggesting the formation of Ag NPs. For the samples co-doped with 1 mol% Nd^{3+} (Fig. 1b), a light purple color emerged, as typically observed for glasses doped with Nd^{3+}.

The DSC thermograms of all samples are presented in Fig. 2. The glass transition temperatures were determined by the onset peak in the range 453–482 °C. A pronounced shift in the DSC baseline observed for all samples indicates the characteristic behavior of structurally "soft" glasses with low network connectivity.[28] The progressive incorporation of Ag resulted in a systematic decrease in T_g, both for Ag and Ag/Nd co-doped samples. This effect is commonly associated with the network-modifying role of Ag^{+} ions, which tends to break P–O–P or Ga–O–P chains, thereby reducing the overall connectivity of the phosphate-fluoride network.[29] The slight increase in T_g observed upon Nd^{3+} addition is indicative of a modest network strengthening effect. A similar trend was reported by Jiménez for Nd^{3+} doped phosphate glasses, where T_g increased systematically with Nd_2O_3 content despite the partial depolymerization of the phosphate network.[30] This behavior was attributed to the higher ionic field strength of Nd^{3+} compared to modifier cations, associated with its smaller ionic radius and higher charge, which promotes stronger Nd–O interactions and increases the rigidity of the glass structure. Such an effect has been widely reported for lanthanide-doped phosphate glasses and is consistent with the thermal behavior observed in the present system.

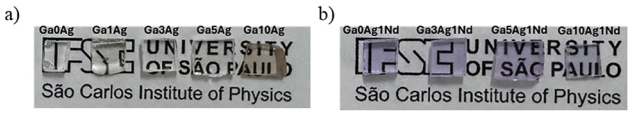

Fig. 1 Glass samples: (a) doped with Ag^{+} (0, 1, 3, 5 and 10 mol%); (b) co-doped with Ag^{+} (0, 3, 5 and 10 mol%) and 1 mol% Nd^{3+}.

Table 2 Characteristic temperatures of the glass samples, measured by DSC

Sample	T_g (°C)	T_x (°C)	T_p (°C)
Ga0Ag	478	653	687
Ga1Ag	476	636	674
Ga3Ag	464	625	672
Ga5Ag	453	654	687
Ga10Ag	453	643	667
Ga0Ag1Nd	480	639	684
Ga3Ag1Nd	469	675	704
Ga5Ag1Nd	455	651	684
Ga10Ag1Nd	460	636	657

The characteristic temperatures are summarized in Table 2. Across the scanned range (100–750 °C), all samples exhibit a single crystallization exotherm, with onset temperatures typically located ~170–200 °C above T_g and peak temperatures between 687 °C and 704 °C. No direct correlation between Ag content or Nd^{3+} co-doping and shifts in T_p could be identified. In rare-earth-doped phosphate glasses, the increase in T_x and improved thermal stability are commonly observed with RE incorporation.[30] In the present system, however, the Nd^{3+} concentration is fixed, and T_x and T_p show only moderate, non-monotonic variations governed by the combined effects of Ag incorporation and Nd^{3+} co-doping. Despite these variations, the relatively large T_x–T_g separation for all compositions indicates good resistance to crystallization.

3.2 Spectroscopic properties

3.2.1 UV-Vis absorption. Fig. 3 presents the UV–Vis–NIR absorption spectra of the synthesized glasses. All the Ag-doped samples exhibit high optical transparency from at least 380 nm up to more than 1000 nm. Increasing silver concentration leads to a shift of the UV cutoff to longer wavelengths, which is attributed to the absorption of Ag^{+}, Ag^{+}–Ag^{+} pairs and Ag NCs.[31] For the 10 mol% Ag glass (Ga10Ag), a broad and low-intensity absorption band appears between 400 and 600 nm, imposing an elevation of the spectral baseline. This feature is tentatively assigned to SPR of Ag NPs (with a broad diameter distribution) formed during the glass quenching. An alternative interpretation,

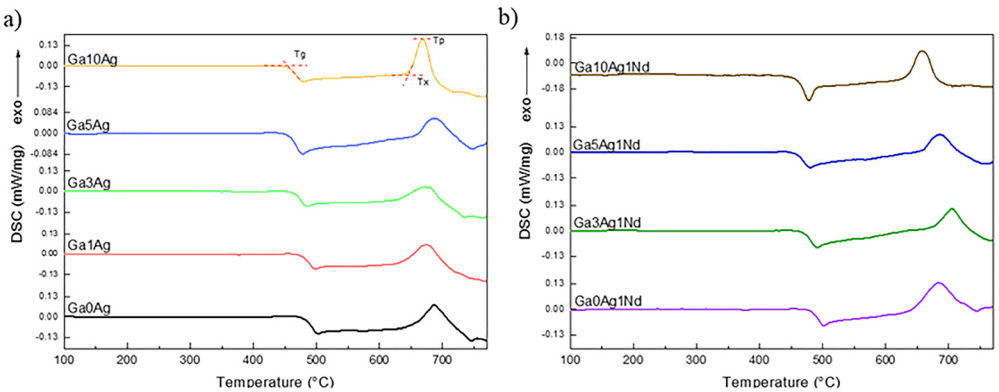

Fig. 2 DSC curves of gallium-FP glasses recorded at 10 °C min^{-1}: (a) Ag-doped samples; (b) Ag/Nd co-doped samples.

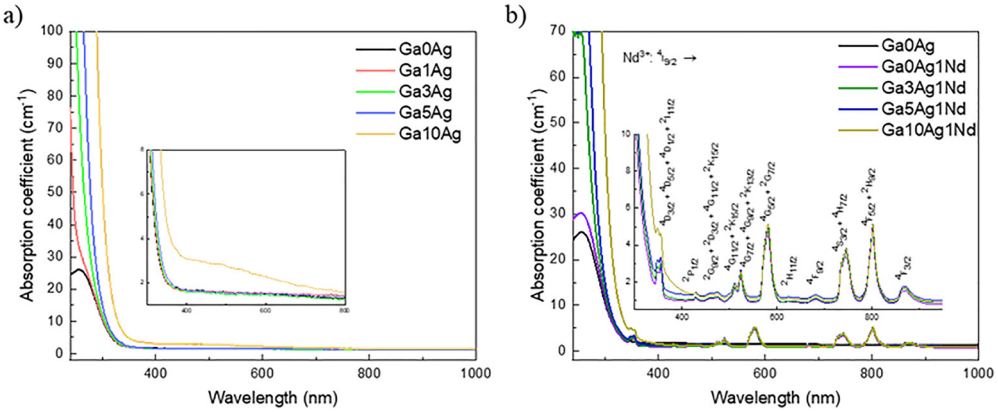

Fig. 3 UV-Vis-NIR absorption spectra of FP samples: (a) Ag-doped; (b) Ag/Nd co-doped. The inset in (b) shows a zoom of Nd^{3+} absorption bands.

and a non-exclusive contributing factor, is the scattering of light caused by the presence of larger Ag-rich domains or particles within the glass. According to Mie scattering theory, such scattering becomes more significant at shorter wavelengths, which would also explain the brownish coloration of this sample (Fig. 1a).[32]

The absorption spectra of Ag/Nd co-doped glasses (Fig. 3b) present additional sharp peaks assigned to the characteristic 4f–4f Nd^{3+} transitions: 355 nm ($^4I_{9/2} \rightarrow {}^4D_{3/2} + {}^4D_{5/2} + {}^4D_{1/2} + {}^2I_{11/2}$), 428 nm ($^4I_{9/2} \rightarrow {}^2P_{1/2}$), 465 nm ($^4I_{9/2} \rightarrow {}^2G_{9/2} + {}^2D_{3/2} + {}^4G_{11/2} + {}^2K_{15/2}$), 510 nm ($^4I_{9/2} \rightarrow {}^4G_{11/2} + {}^2K_{15/2}$), 524 nm ($^4I_{9/2} \rightarrow {}^4G_{7/2} + {}^4G_{9/2} + {}^2K_{13/2}$), 581 nm ($^4I_{9/2} \rightarrow {}^4G_{5/2} + {}^2G_{7/2}$), 623 nm ($^4I_{9/2} \rightarrow {}^2H_{11/2}$), 681 ($^4I_{9/2} \rightarrow {}^4F_{9/2}$), 676 nm ($^4I_{9/2} \rightarrow {}^4S_{3/2} + {}^4H_{7/2}$), 802 nm ($^4I_{9/2} \rightarrow {}^4F_{5/2} + {}^2H_{9/2}$) and 869 nm ($^4I_{9/2} \rightarrow {}^4F_{3/2}$).[33]

The 10 mol% Ag^+ and 1 mol% Nd^{3+} co-doped glass (Ga10Ag1Nd) also presents a baseline elevation (as seen for Ga10Ag), particularly in the short-wavelength region (<450 nm), although less pronounced than that observed for Ga10Ag. Importantly, no distinct surface plasmon resonance band can be resolved for either composition. The observed spectral behavior is more consistently attributed to light scattering associated with silver-rich heterogeneities rather than to plasmonic absorption.

3.2.2 Photoluminescence spectroscopy. The undoped fluoride-phosphate glass (Ga0Ag) was evaluated under different excitation wavelengths (300 and 355 nm), and no detectable emission was observed (Fig. S1 in the Supporting Information). The glass matrix is thus optically inactive in the studied range, so that all the spectroscopic features hereafter discussed are induced by Ag species and/or Nd^{3+} ions.

To follow the PL response and the evolution of Ag species upon heat treatment, excitation and emission spectra were recorded before and after annealing for 4 h at 50 °C below the corresponding T_g value. Fig. 4 shows the emission and excitation spectra for the 5 mol% Ag^+ doped sample (Ga5Ag). Prior to annealing, excitation at λ_{exc} = 260 nm, leads to a broad emission band centered at 390 nm, attributed to isolated Ag^+ ions; for λ_{exc} = 300 nm, the center of this band shifts to 437 nm; and for λ_{exc} = 355 nm, it shifts to 506 nm. This broadband emission suggests the presence of a few small silver NCs Ag_2^+ or ion pairs Ag^+–Ag^+.[34,35] Nevertheless, the spectral positions and relative intensities of bands are highly dependent on the glass

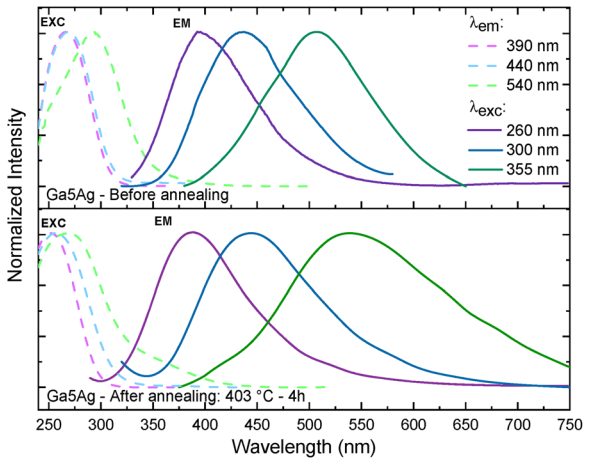

Fig. 4 Excitation and emission photoluminescence spectra of the Ga5Ag sample before and after annealing at 50 °C below T_g (403 °C) for 4h.

composition and on the local environment of Ag species. Therefore, the assignments are proposed with caution, based on comparative trends previously reported in literature.[27,31,34,36]

After annealing, only minor spectral changes are observed for λ_{exc} = 260 nm, with the 390 nm band being preserved. Under excitation at 300 nm, a broad band appears at around 440 nm which can be ascribed to the formation of small NCs, most likely Ag_2^+. The small spectral shift relative to the pre-annealed glass state suggests that these small NCs show relatively stable bonds that are weakly affected by the thermal treatment. In contrast, excitation at 355 nm leads to a much broader band covering almost the entire visible range and centered around 540 nm. This pronounced redshift in respect to the pre-annealed sample indicates the contribution of Ag^+–Ag^+ ion pairs may exist in a wider distribution of local environments, thus leading to emissions more sensitive to the structural relaxation and microscopic rearrangements induced by annealing.[34,35] This observation is in agreement with the reports by Ma *et al.*,[31] which claim that the broadband emission of Ag-doped oxyfluoride glasses are due to multiple Ag-related centers. More specifically, the broadband centered at ~390 nm

is assigned to electronic transitions in isolated Ag^+ ($4d^95s^1 \rightarrow 4d^{10}$), while the bands at ~440 and ~540 nm are associated with small NCs and ions pairs, respectively. These transitions are mostly singlet → singlet or triplet → triplet spin-allowed ones but spin-forbidden transitions may also occur.

The excitation spectra of Ga5Ag show a consistent behavior with the emission data. Prior to annealing and by monitoring the emissions at 390 and 440 nm, the excitation band is centered at 260 nm, whereas for the emission at 540 nm a pronounced redshift of excitation is observed to 290 nm. After annealing and polishing, a broad excitation band centered near 270 nm appears when emissions are monitored at 390, 440, and 540 nm, together with a weaker band around 330 nm. This spectral evolution corroborates the hypothesis of thermally induced Ag species (ions, Ag^+–Ag^+ pairs and small NCs).[34,35]

Fig. 5 presents the emission/excitation spectra of Ga10Ag. In contrast to Ga5Ag two overlapped emission features are already evident before annealing and optical polishing, centered around 390 and 460 nm (λ_{exc} = 260 nm), 400 and 460 nm (λ_{exc} = 300 nm), and 400 and 560 nm (λ_{exc} = 355 nm). These pre-annealing spectra all show an inflection around 420 nm likely due to inner-filter effect (reabsorption) due to the overlap with the SPR band of Ag NPs. The persistence of this feature after annealing confirms the formation of Ag-NPs already at the melting and quenching stages at the Ga10Ag glass surface. This conclusion is supported by the fact that after polishing the annealed sample, this effect vanishes, and the resulting emission spectra resemble those of Ga5Ag, with bands centered at 390 nm (λ_{exc} = 260 nm), 460 nm (λ_{exc} = 300 nm), and 540 nm (λ_{exc} = 355 nm).

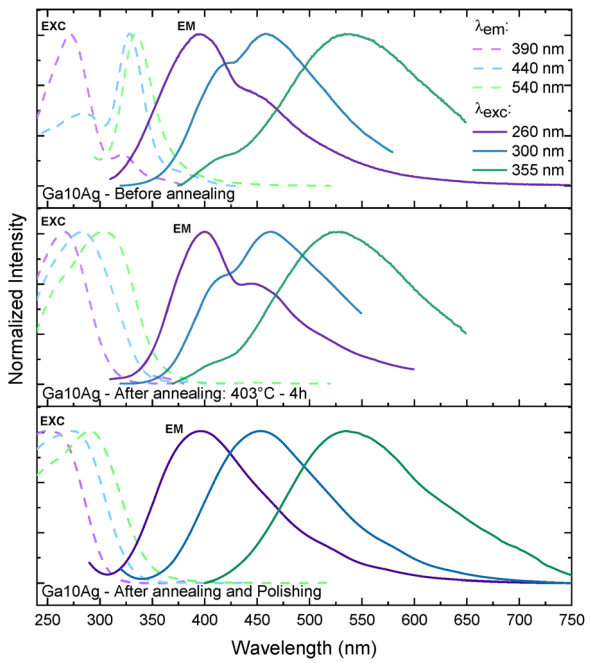

Fig. 5 Excitation and emission photoluminescence spectra of the Ga10Ag sample before, after annealing at 403 °C for 4h and after polishing.

The excitation spectra of Ga10Ag evolve similarly to Ga5Ag. Before annealing and polishing, a contribution around 330 nm is observed, consistent with the presence of silver NCs.[36] In line with the observations by Belharouak *et al.*[35] the coexistence of Ag^+–Ag^0 centers near metallic particles or at the glass–metal interface may account for this contribution. Consequently, once these surface nanoparticles are removed by polishing, the 330 nm band disappears, indicating that both the NC-related and metallic species were predominantly located close to or at the glass surface.

The standardized annealing protocol (heating at 50 °C below T_g, for 4 h) was applied to all samples and a comparison of their excitation and emission spectra is given in Fig. S2. The results show the expected trend and features associated to the co-existence of Ag^+ ions, Ag_2^+ NCs and Ag^+–Ag^+ pairs in the glasses. Ma *et al.*[31] further argued that the presence of silver ions stable pairs, in fluoride-rich hosts containing BaF_2, ZnF_2, and SrF_2, inhibits both the growth of larger nanoclusters and the nucleation of metallic silver NPs. This observation highlights the balance between cluster stabilization and NP formation inside of glass, ruled by local coordination and redox conditions.

Fig. 6 presents photographs of the undoped and Ag-doped samples after annealing an polishing, being excited at different wavelengths, along with the corresponding CIE chromaticity diagrams. Upon excitation at 260 and 300 nm (Fig. 6b and c), all doped samples present a blue emission typical of Ag^+, most prominent for 1 mol%. At 355 nm (Fig. 6d) the overall emission of 3, 5, and 10 mol% samples shift towards greenish white. Under 400 nm excitation (Fig. 6e), Ga5Ag and Ga10Ag emit yellow light, while Ga3Ag emits warm yellowish white. Thus, emission color can be tuned by selecting the excitation wavelength across the series, a behavior linked to the relative weight of Ag^+, Ag^+–Ag^+ pairs and Ag-NCs. This tunability underscores the versatility of Ag-doped systems and paves the way for the following discussions on the additional effects arising from Nd^{3+} co-doping.

For the sake of comparison, the concentration of Nd^{3+} was fixed at 1 mol% and the excitation and emission behaviors were characterized in the visible and NIR spectral regions (Fig. 7 and 8, respectively). For Ga0Ag1Nd under 355 nm excitation (Fig. 7a), two weak narrow emissions arise at 415 and 450 nm, due to Nd^{3+} 4f–4f transitions. At this excitation wavelength, both the Nd^{3+} ions and the glass matrix are excited, as I t is seen by the presence of the overlapping tail of the matrix (spectrum in purple).

On a first approach, the spectra of Ag/Nd co-doped samples (Fig. 7b–d) display the characteristic previously discussed broadband emission of Ag^+ and Ag^+–Ag^+ pairs. However, distinctive intensity dips are superimposed to these broad bands at 428, 475, 510, 524, and 575 nm that coincide with Nd^{3+} absorption lines (Fig. 3b). This is a clear indication that part of the emission of the Ag species is absorbed by Nd^{3+}.[37] The magnitude of these dips depends on both Ag concentration and excitation wavelength. For a given Ag content, excitations with shallower penetration, such as 355 nm, produce less pronounced reabsorption distortions than deeper-penetrating

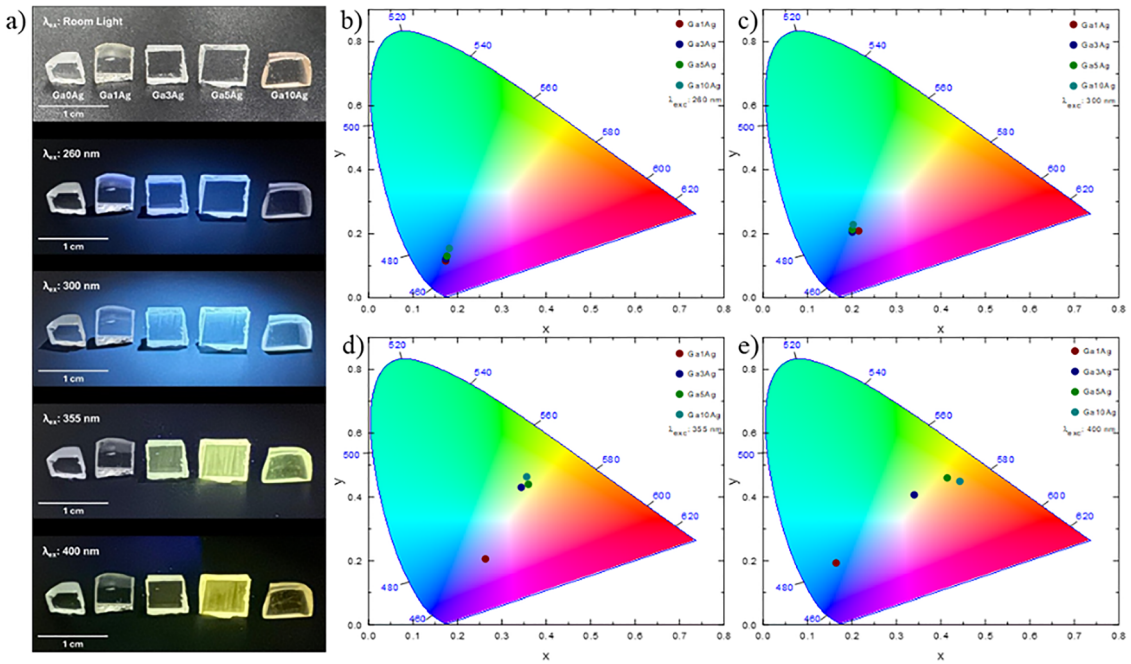

Fig. 6 (a) Photographs of undoped and Ag-doped samples under different excitation wavelengths; (b–e) CIE 1931 chromaticity diagrams of the doped samples.

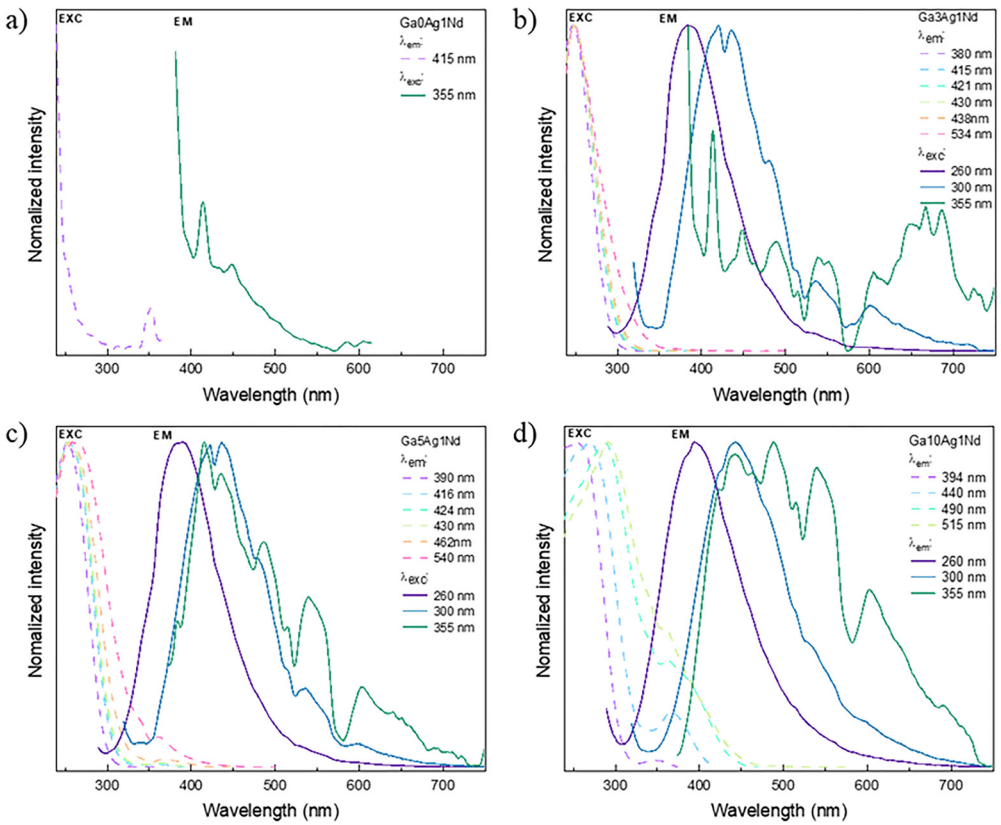

Fig. 7 Excitation and emission photoluminescence spectra in the visible of FP glasses doped with 1 mol% Nd^{3+} and variable Ag^{+} concentrations: (a) 0 mol%, (b) 3 mol%, (c) 5 mol%, and (d) 10 mol%.

UV excitations, which is consistent with a shorter propagation path for the Ag emission prior to collection.

To further investigate the interplay between Ag species and Nd^{3+} ions in the co-doped FP glasses, the emission was also

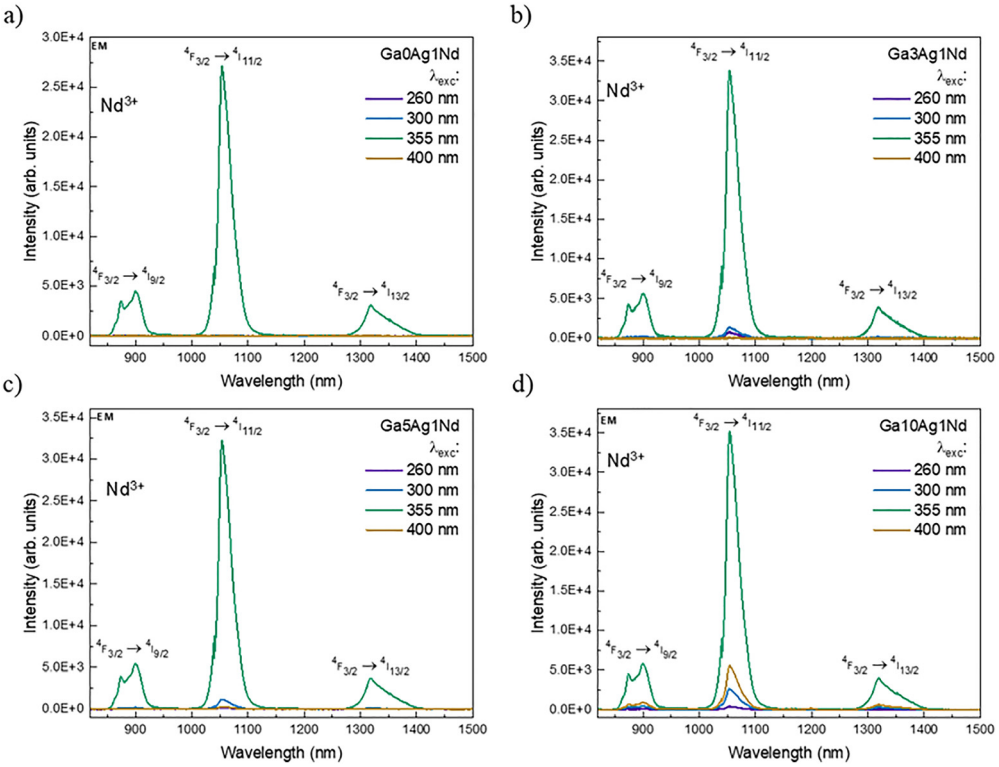

Fig. 8 Near-IR emission spectra of FP glasses doped with 1 mol% Nd^{3+} and different Ag^{+} concentrations: (a) 0 mol%, (b) 3 mol%, (c) 5 mol%, and (d) 10 mol%.

analyzed in the near-IR 800–1500 nm region (Fig. 8). The emission lines arise solely from Nd^{3+} ions and are centered at 900, 1053, and 1315 nm, corresponding to the $^4F_{3/2} \rightarrow {}^4I_{9/2}$, $^4F_{3/2} \rightarrow {}^4I_{11/2}$, and $^4F_{3/2} \rightarrow {}^4I_{13/2}$ transitions, respectively. For Ga0Ag1Nd (Fig. 8a), these bands are only detected when the Nd^{3+} ion is directly excited at 355 nm. For Ag containing glasses, excitations at 260, 300, and 400 nm also led to a Nd^{3+} emission. Similar observations have been made and reported for phosphate and fluoride-based glasses doped with rare-earth ions (*e.g.* Eu^{3+}, Yb^{3+}) where, besides reabsorption, non-radiative phonon-assisted transfers from Ag^{+} or NCs to the RE ions also lead to indirect excitation of the rare earth ion.[7,16]

By monitoring the emission at 1053 nm, the excitation spectra (Fig. 9a) show that, besides the Nd^{3+} lines around 330 and 350 nm, a broad UV contribution below 300 nm appears in Ga3Ag1Nd, proving the Ag^{+} sensitization. In Ga5Ag1Nd, this Ag^{+} signature is weaker, in agreement with the higher prevalence of Ag^{+}–Ag^{+} pairs. For Ga10Ag1Nd, a broader feature from 300 to beyond 400 nm also contributes to Nd^{3+} sensitization, which can be tentatively attributed to NCs.[36] Because the excitation bands of NCs and Ag^{+}–Ag^{+} pairs overlap, time-resolved measurements are required for an unambiguous assignment.

Fig. 9b presents a comparison of the emission spectra of the co-doped samples excited at 355 nm. Although the comparison

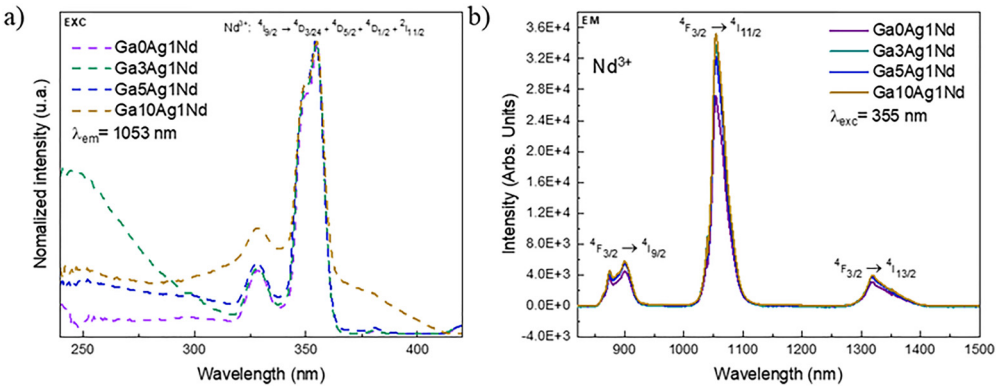

Fig. 9 (a) Normalized excitation spectra of Ag/Nd co-doped samples with 0, 3, 5, and 10 mol% Ag^{+}, monitored at 1053 nm; (b) emission spectra under excited at 355 nm.

of intensities is not strictly correct, we take this approach solely in search for a trend, having secured that the samples had the same thickness and position in the fluorimeter. Under these conditions, a progressive intensity increase at 1053 nm is detected with increasing Ag^+ concentration. The 10 mol% doped sample shows approximately 1.3-fold intensity enhancement as compared to the Ag-free sample, corroborating the sensitization role of Ag species under various forms and *via* different pathways (energy transfer and re-absorption).

3.2.3 Time-resolved photoluminescence. To gain deeper insight into the nature of the interaction between Ag-species and Nd^{3+} in the FP glasses, time-resolved photoluminescence measurements were performed upon 300 nm excitation, where ionic silver centers are efficiently excited. The decay dynamics were monitored at 500 nm, corresponding to the broad visible emission band associated with Ag^+ and Ag^+–Ag^+ in the glass hosts. The goal was to determine whether the emission decay dynamics of Ag-species are altered by the presence of Nd^{3+}, in order to confirm non-radiative energy transfer besides radiative reabsorption. The decay curves of Ag-doped and Ag/Nd co-doped samples were fitted using a bi-exponential function, reflecting the coexistence of multiple radiative and non-radiative relaxation pathways commonly observed in disordered glassy matrices. Average lifetime values τ_{avg} were calculated, according to the weighted eqn (1):

$$\tau_{avg} = \frac{A_1\tau_1 + A_2\tau_2}{A_1 + A_2} \quad (1)$$

The results are presented in Fig. 10, for samples doped and co-doped with 3, 5 and 10 mol% Ag and 1 mol% Nd^{3+}, while the complete set of decay curves for all Ag-only compositions (0, 1, 3, 5 and 10 mol%) is provided in the Supplementary Information (Fig. S3), allowing direct comparison of the decay behavior as a function of Ag concentration. The fitting parameters and average lifetimes for all samples are summarized in Table S1.

The assignment of each of the two fitted lifetimes to identified and dedicated silver species cannot be certified. Still, the sample Ga3Ag exhibits an average lifetime of 26.4 μs, which decreased significantly to 11.1 μs upon co-doping with Nd^{3+} in Ga3Ag1Nd. Similar behavior was observed for the 5 mol% and 10 mol% Ag-doped samples, where τ_{avg} dropped from 19.7 μs to 8.7 μs, and most significantly from 12.5 μs to 1.4 μs, respectively. The reduction fraction of the average lifetime is thus drastic, corresponding to 58%, 56% and up to 89% for Ga3Ag, Ga5Ag and Ga10Ag, respectively. This consistent reduction in Ag-species lifetime values in the presence of Nd^{3+} gives irrefutable evidence of non-radiative energy transfer from the Ag-species (most likely isolated or paired ions) to RE ions, in addition to the radiative reabsorption channel previously discussed.[34,38]

Lifetimes values in the microsecond range are characteristic of isolated Ag^+, Ag^+–Ag^+ pairs, and possibly Ag^+–Ag^0 dimers in phosphate-based hosts.[38] The observed biexponential behavior matches the kinetic model of Velázquez *et al.*[39] with contributions from spin-allowed (fast decay) singlet to singlet or triplet to triplet, and spin-forbidden (slow decay) singlet to triplet channels. Upon Nd^{3+} co-doping, both the fast and slow components tend to decrease and the relative weight shifts toward the short component, driving the decrease of τ_{avg} without implying suppression of the long-lived channel.

It is important to note that, due to the structural disorder of the glass matrix and the strong spectral overlap among different Ag-related centers, a unique assignment of each decay component to a specific silver species (*e.g.*, isolated Ag^+, Ag^+–Ag^+ pairs, or nanoclusters) cannot be made unambiguously. Moreover, the relative contribution of these species is known to depend on both excitation and emission wavelengths. Therefore, the lifetime analysis is treated here in a phenomenological and comparative manner, with emphasis on the evolution of the decay dynamics upon Nd^{3+} co-doping rather than on the precise microscopic identification of individual Ag centers.

Ag-NCs typically exhibit emission lifetimes in the nanosecond regime and are not resolved within the present microsecond time window. Consequently, the measured decay dynamics are attributed predominantly to ionic Ag-related species. In addition, the lifetime of the Nd^{3+} near-infrared emission was directly investigated by monitoring the $^4F_{3/2} \rightarrow {}^4I_{11/2}$ transition at 1051 nm. Decay curves were recorded under both indirect excitation at 300 nm, selectively exciting Ag-related centers, and direct excitation of Nd^{3+} at 355 nm. The corresponding decay curves are presented in Fig. S4, and the fitting parameters are summarized in Table S2. In all cases, the Nd^{3+} emission exhibits a predominantly single-exponential behavior with lifetimes in the range of ~310–330 μs for

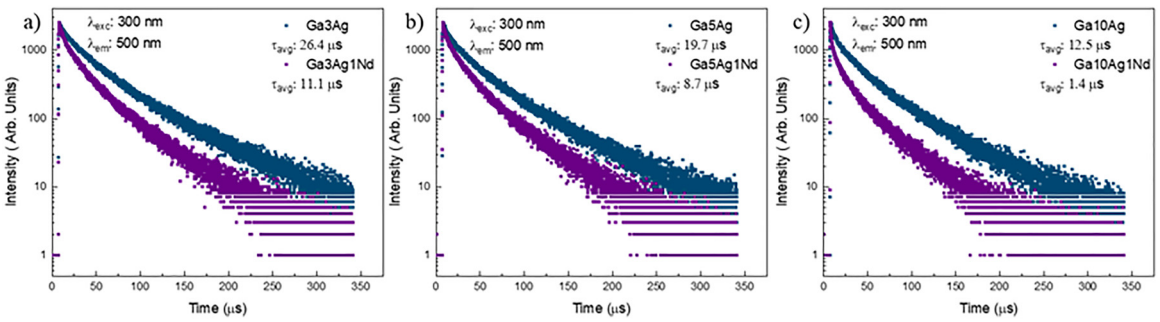

Fig. 10 Time-resolved emission decay curves of FP glass samples singly Ag-doped or Ag/Nd co-doped, under 300 nm excitation and monitoring the emission at 500 nm: (a) 3 mol% Ag^+, (b) 5 mol% Ag^+, and (c) 10 mol% Ag^+.

Ga0Ag1Nd, Ga3Ag1Nd and Ga5Ag1Nd, values that are fully consistent with those reported in the literature for Nd^{3+} ions in phosphate-based glass hosts.[40] Moreover the results are corroborated by the role of ionic Ag species as effective sensitizers for Nd^{3+}, with no appreciable impact on the Nd^{3+} emission lifetime.

3.3 Direct laser writing and characterization by FLIM

Direct laser writing was used in order to spatially control the formation of Ag NCs so as to provide a 3D high optical contrast for near-IR fluorescence emission. This was applied to FP samples doped with 3 and 5 mol% Ag^{+} and co-doped with 1 mol% Nd^{3+}. Ga10Ag and Ga10Ag1Nd samples showed excessive background emission and material degradation prevented laser inscription. Linear tracks of 50 μm in length were inscribed by varying the laser intensity (3.86, 4.22, and 5.57 TW cm^{-2}), scanning speed (10, 50, and 100 μm s^{-1}), and number of passes (1 and 5). These parameters were chosen to evaluate the influence of energy deposition on the formation and distribution of Ag-NCs.

Fig. 11 presents UV-light (λ_{exc} = 365 nm) wide-field fluorescence micrographs of the laser-written lines in samples Ga3Ag1Nd and Ga5Ag1Nd. Ga5Ag1Nd (Fig. 11b) shows clearly a significantly brighter tracks as well as a brighter diffuse background fluorescence of unprocessed regions. In contrast, Ga3Ag1Nd (Fig. 11a) exhibits well-defined bright lines with minimum background emission, indicating that laser-induced Ag species are more dominantly localized within the laser-modified zones, as compared to the pristine glass.

This behavior reflects the higher concentration of Ag-related luminescent species in the pristine 5 mol% sample, which are broadly distributed throughout the matrix and contribute to a non-negligible baseline emission. Despite of that, the laser-inscribed lines in Ga5Ag1Nd appear brighter than those in Ga3Ag1Nd due to the higher availability of Ag ions, thus enhancing the formation of luminescent NCs in the irradiated regions. Besides, an increase in fluorescence intensity is evident for lines written at higher laser intensity, highlighting the role of laser energy in enhancing NC formation.

In order to probe the spectroscopic characteristics of the laser written regions, emission spectra were collected under excitation at 405 nm. The signal was not corrected for the spectral response of the micro-spectrometer. Since both singly and co-doped samples with 3 and 5 mol% Ag exhibited similar spectral behavior at identical inscription conditions (Fig. S5), only the results for the 5 mol% sample are shown.

For the Ga5Ag sample (Fig. 12a), a broad visible emission band centered around 500 nm is observed, consistent with the characteristic luminescence of Ag_m^{x+} NCs. Spectral recording is achieved under confocal microscope collection so that the involved emissive Ag_m^{x+} NCs are exclusively those created by DLW, as proved by the absence of background emission from the pristine glass. Such an emission band (Fig. 12a) differs from that in Fig. 4 since highly localized laser-induced NCs (and associated PL) differ from the low-concentration randomly distributed pre-existing silver NCs in the glass. Such an assignment is further supported by the ns decay dynamics, typical of Ag-NCs lifetimes.[7,16,22,23,35] This emission profile closely resembles the steady-state emission measured before laser irradiation and agrees with previous reports on Ag-doped oxide glasses, where such broadband emission was attributed to mixed Ag NC species.[27,36]

In contrast, the co-doped Ga5Ag1Nd sample (Fig. 12b) exhibits a slight blue shift of the broadband emission, centered at 490 nm. Additionally, the first emission band of Nd^{3+} appears at around 880 nm. The broadband shifting of the NC emission suggests that the presence of Nd^{3+} influences the laser–material interaction. Our assumption is that Nd^{3+} absorbs part of the laser energy (leading to a slightly lower local peak intensity) or affects the local field and Ag ion mobility during cluster formation, leading to the creation of smaller and/or fewer Ag species. Still, spectra from Fig. 12(a) of Ga5Ag were checked to be homothetic to the others, so that no spectral distortion was observed for the NC emission (it is also the case for spectra from Fig. 12b with Ga5Ag1Nd, both, for the NC and Nd^{3+}emissions). Contrary to Fig. 7b–d that correspond to a macroscopic response, no visible-range reabsorption dips associated with Nd^{3+} absorption are observed under confocal microscopy of the laser-inscribed structures (typical thickness of 5–10 μm located at 150 μm below the glass surface). Besides, one observes a clear distortion of the NIR Nd^{3+} emission around 880 nm in laser-inscribed areas (Fig. 12b) compared to the pristine glass emission (Fig. 8 and 9b), suggesting a significantly distinct environment of Nd^{3+} ions in presence of the laser-induced

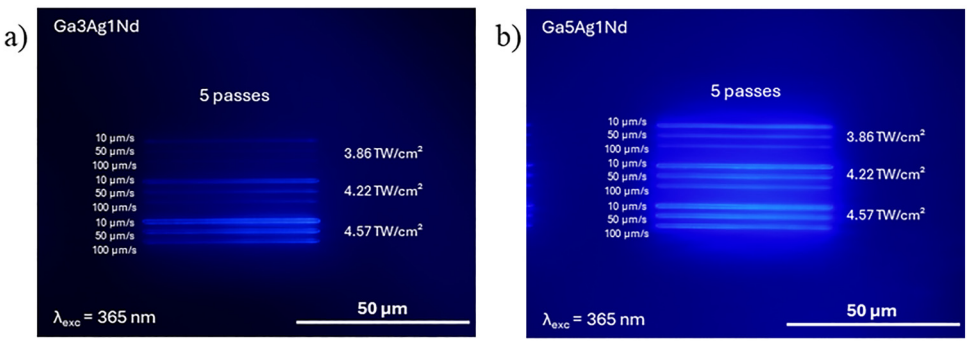

Fig. 11 Fluorescence images (λ_{exc} = 365 nm, 60 ×/0.7 NA objective) of laser written lines in samples: (a) Ga3Ag1Nd; (b) Ga5Ag1Nd.

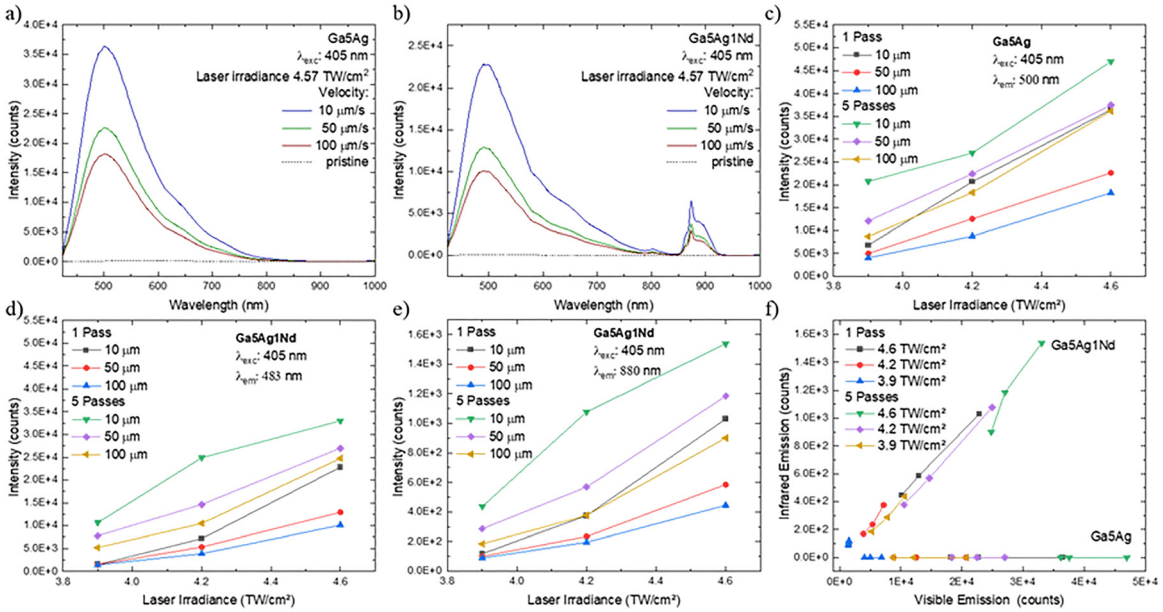

Fig. 12 Microluminescence spectra of laser written lines under 405 nm excitation for (a) Ga5Ag and (b) Ga5Ag1Nd (both single pass DLW); peak intensity of Ag-NC visible emission *versus* laser irradiance for (c) Ga5Ag and (d) Ga5Ag1Nd; (e) peak intensity of Nd^{3+} emission at 880 nm in Ga5Ag1Nd; (f) correlation between Ag-NC visible emission and Nd^{3+} emission (NIR) in Ga5Ag1Nd by combining (d) and (e).

silvers NCs. Alternatively, the spectra in Fig. 12b may be less affected than those in Fig. 8 and 9b by reabsorption and typical spectral redshift (*e.g.* similarly to Yb^{3+} emission in thick samples).

When comparing the influence of laser irradiation parameters, a clear trend emerges. At lower scanning speeds (more cumulated laser pulses) higher fluorescence intensities are measured for both the broadband visible and Nd^{3+} NIR emissions. The background emission of pristine glass areas show that both the visible and NIR emissions are negligible (below 100 counts for the Nd^{3+} emission at 880 nm). This NIR background-free emission confirms that Nd^{3+} ions are not directly excited at 405 nm (see Fig. 3b, 8 and 9a). Thus, the laser-induced formation of Ag NCs appears crucial for the observed sensitization, leading to remarkably high 3D-localized optical contrast of both NC visible emission and NIR Nd^{3+} emission excited *via* energy transfer from Ag NC. Hence, this approach allows highly localized NIR emission (co-localized with Ag NCs), despite the NIR emitters being randomly distributed in the whole sample. Spatially localized energy transfers thus allow the spatially-selective excitation of emitters in patterns produced on-demand by DLW, opening an interesting route for the creation of laser-active photonic circuits with highly localized excitation ability of the gain medium.

To better understand the influence of inscription parameters, a micro-luminescence mapping experiment was conducted across a section containing all the written lines. The resulting data are plotted in Fig. 12c–f. In Fig. 12c the peak intensities from the Ga5Ag glass were plotted for each writing condition (number of passes and laser irradiance). As shown, the intensity increases with laser power and with multiple passes but decreases with faster writing speeds. Although the cumulative effect of five passes does not yield a five-fold increase in intensity, it results in approximately 3-fold enhancement, suggesting a partial saturation of silver cluster formation that results from the significant use of the available Ag^{+} ions. This interpretation is in line with that of Desmoulin *et al.*[41] who had shown that DLW induces Ag ion migration and redistribution in phosphate glasses, leading to the consumption of available Ag^{+} in the irradiated voxel and to the formation of luminescent clusters at its periphery.

A similar behavior is observed for Ga5Ag1Nd (Fig. 12d). While the overall visible emission is lower in comparison to Ga5Ag, the same trends with power, speed, and pulse accumulation are evidenced. Furthermore, the Nd^{3+} emission at 880 nm (Fig. 12e) follows the same trend. Finally, Fig. 12f correlates the visible emission from laser-inscribed silver NCs and the co-localized Nd^{3+} NIR emission. The nearly linear relationship between these two signals confirms that the enhancement of Nd^{3+} emission directly links to the formation and optical activation of NCs in irradiated regions.

The energy transfer from NCs to Nd^{3+} was further investigated by confocal FLIM imaging in Fig. 13a and b for Ga5Ag and Ga5Ag1Nd, respectively). Excitation was performed at 405 nm and collection covered the 470–550 nm range to selectively probe the fluorescence of Ag NCs. As discussed in Fig. 12, such an approach under microscope is free from Nd^{3+} re-absorption effects, so that any radiative energy transfers can be disregarded which allows for consider only non-radiative energy transfers. Fig. 13a and b display double-scale images combining an intensimetric scale (grey) and a lifetime (colorimetric) scale, revealing the well-defined laser-written fluorescent patterns corresponding to the spatial distribution of Ag NCs within the glass.

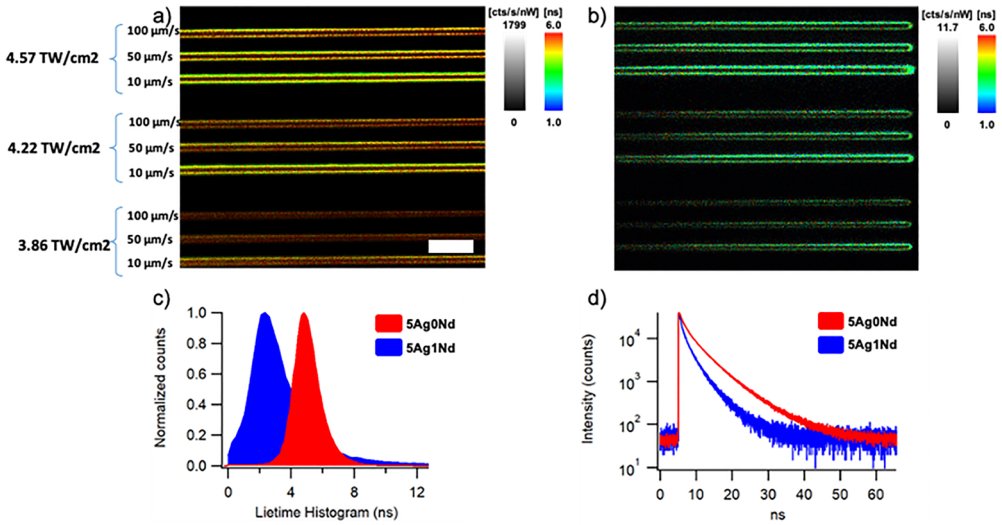

Fig. 13 Confocal FLIM images of laser-inscribed patterns in (a) Ga5Ag and (b) Ga5Ag1Nd (λ_{exc} = 405 nn, λ_{em} = 470–550 nn). Color scales represent the average lifetime value of each pixel obtained from FAST-FLIM method, and grey scales represent the photon count rates per pixel (rate normalized by the excitation intensity). Scale bar: 10 µm. (c) Intensity-weighted distributions of pixel lifetime values corresponding to images (a) and (b), normalized to the peak value. (d) Fluorescence decays obtained from the summation of all pixels from images (a) and (b), normalized to the peak value.

A clear dependence of fluorescence intensity and lifetime with DLW parameters is observed for each glass (irradiances of 3.86 TW cm^{-2}, 4.22 TW cm^{-2} and 4.57 TW cm^{-2}, and speeds of 100 µm s^{-1}, 50 µm s^{-1} and 10 µm s^{-1}). The intensimetric scales also show a very strong difference of intensity, with a typical 150-fold decrease in the fluorescence of Ag-NCs in Ga5Ag1Nd as compared to Ga5Ag. This indicates that the presence of Nd^{3+} ions contributes to the quenching of the NCs emission and/or to limit their presence during the DLW process. The lifetime map also shows parameter-dependent variations, but the prominent effect is a global shortening of the mean lifetime in the co-doped sample (orangish *versus* greenish color for Ga5Ag and Ga5Ag1Nd, respectively), demonstrating an efficient energy transfer from Ag-NCs to Nd^{3+} ions.

To quantify this effect, intensity-weighted lifetime histograms were extracted from Fig. 13a and b and are shown in Fig. 13c. For clarity, both distributions were normalized to unity, although the overall signal from Ga5Ag1Nd is significantly weaker, 150-fold lower than that of Ga5Ag, in agreement with the intensity maps. The histograms peak at 4.80 ns for Ga5Ag and 2.36 ns for Ga5Ag1Nd, confirming the lifetime reduction. The ensemble decays derived from the same datasets are shown in Fig. 13d, which clearly displays a faster temporal decay of the laser-inscribed NCs in presence of Nd^{3+} ions. Fitting these decays with a triple-exponential model brings three weight/time couples $\{A_{i=1,2,3};\tau_{i=1,2,3}\}$ given in Table S.3, giving access to the overall amplitude-weighted mean lifetimes $\tau_{Ag}^{av} \sim 3.19$ ns and $\tau_{Ag1Nd}^{av} \sim 1.76$ ns, corresponding to a 45% lifetime quenching ratio $Q(\tau_{5Ag1Nd}^{av}/\tau_{5Ag}^{av}) = 1 - \tau_{5Ag1Nd}^{av}/\tau_{5Ag}^{av}$. This substantial reduction is due to the strong nonradiative energy transfer between Ag NCs and Nd^{3+} in these FP glasses, comparable to quenching ratios previously reported for Eu–Ag (27%),[7] Ag–Yb (15%)[22] and Ag–Bi (56%)[23] glasses.

To go beyond the overall image analysis of mean fluorescence lifetime of Fig. 13d, energy transfers and quenching ratios are investigated in detail for each irradiation condition.

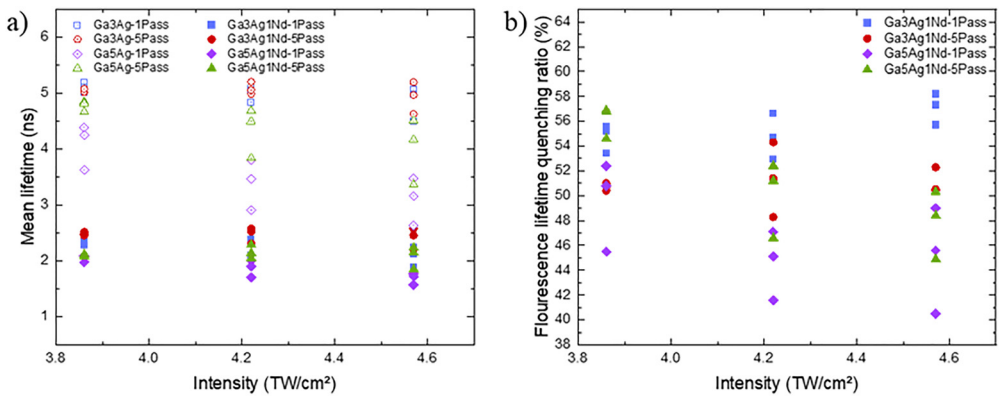

Fig. 14 (a) Mean fluorescence lifetimes for the distinct nine laser irradiation conditions for both the 5Ag and 5Ag1Nd glasses; (b) associated fluorescence quenching ratios for the nine laser irradiation conditions. Evaluation based on the independent analysis of each laser-inscribed patterns from Fig. 13a and b.

Fig. 13a and b were thus locally processed for each laser-inscribed pattern, rather than averaged over the entire image. Temporal decay behaviors with/without Nd^{3+} were extracted and fitted (same three-exponential decay model) for each laser irradiation condition, leading to the determination of irradiation dependent values: (i) the fitted parameters $\{A_{i=1,2,3};\tau_{i=1,2,3}\}$; (ii) the average lifetimes τ^{av}_{5Ag} and τ^{av}_{5Ag1Nd} (Fig. 14a); and the resulting quenching ratios (Fig. 14b). Associated values are summarized in Table S.4.

Both figures confirm that efficient non-radiative energy transfers take place for all the nine patterns associated to distinct laser-irradiation conditions, proving the systematic mean average lifetime shortening of laser-inscribed Ag-NCs in presence of Nd^{3+} ions. The associated detailed quenching ratios range between 35% and 55%, in agreement with the mean value of 45% estimated from Fig. 13d.

4. Conclusions

In this work, we developed and characterized novel gallium fluoride-phosphate glasses singly doped with silver and co-doped with Nd^{3+}. Silver can be stabilized in the glass matrix in different ionic and molecular species such as Ag^{+}, Ag^{+}–Ag^{+} pairs and Ag nanoclusters. These species exhibit overlapping emissions resulting in a broad spectral band over the visible range. Samples co-doped with Nd^{3+} present, additionally to the silver features, narrow emission peaks in the NIR whose intensities are substantially enhanced by energy transfer from the Ag species, as confirmed by steady-state and time-resolved experiments. Direct laser writing proved to be a powerful tool to control the localized formation of Ag NCs. The laser-inscribed regions exhibited enhanced luminescence of both co-localized Ag NCs (with ns lifetime) and Nd^{3+} ions, depending on laser inscription parameters. Background-free NIR emission could be selectively excited in such laser-inscribed regions over the excitation range of the co-localized laser-inscribed silver NCs. This led to a nearly linear correlation between emissions of NCs and Nd^{3+} in the structured areas, which reinforces the idea of localized non-radiative energy transfers, demonstrating how DLW can be an effective strategy to spatially design luminescent and, potentially, laser-active responses. Altogether, the study shows that fluoride-phosphate glasses are promising optical materials in which the combination of DLW, Ag NCs and RE^{3+} enables the development of photonic devices for displays, high-density 3D optical data storage, optical standards for the calibration of visible/NIR confocal microscopes, and miniaturized light sources.

Conflicts of interest

There are no conflicts to declare.

Data availability

All data supporting the findings of this study are included within the article and its supplementary information (SI). Further details can be obtained from the corresponding author upon reasonable request. Supplementary information is available. See DOI: https://doi.org/10.1039/d5ma01430a.

Acknowledgements

This work was supported by the São Paulo Research Foundation (FAPESP, Brazil) through the following grants: 2021/14705-2 (PhD scholarship of VDJ), 2022/11274-3 (BEPE scholarship of VDJ), 2013/07793-6 (CEPID program), 2021/08111-2 (Thematic Project), 2024/15684-7, and 2024/02102-0 (Postdoctoral fellowships of LGM). The authors are also grateful to Prof. André Del Guerzo for providing access to the FLIM instrumentation. This research was additionally supported by the Agence Nationale de la Recherche (ANR) under grants ANR-23-CE08-0021 and EUR LIGHT S&T PIA3 (ANR-17-EURE-0027), by the New Aquitaine Region (AAPR2024I-2023-32376110; AAPR2020-2019-8193110), and by the ANR ''Investissements d'avenir'' program (ANR-10-IDEX-03-02).

References

1 G. Galleani, C. Doerenkamp, S. Santagneli, C. J. Magon, A. S. S. de Camargo and H. Eckert, *J. Phys. Chem. C*, 2019, **123**, 31219–31231.
2 A. Gaddam, G. Galleani, V. de Lima Reis, A. S. S. de Camargo and H. Eckert, *J. Am. Ceram. Soc.*, 2024, **107**, 8624–8637.
3 D. Möncke and H. Eckert, *J. Non-Cryst. Solids:X*, 2019, **3**, 100026.
4 S. Cui, J. Massera, M. Lastusaari, L. Hupa and L. Petit, *J. Non-Cryst. Solids*, 2016, **445–446**, 40–44.
5 Z. Yu, W. K. Chan and T. T. Y. Tan, *Small*, 2020, **16**, 1905265.
6 J. C. G. Bünzli, *Coord. Chem. Rev.*, 2015, **293–294**, 19–47.
7 Y. Petit, G. Galleani, G. Raffy, J. C. Desmoulin, V. Jubéra, A. Del Guerzo, A. S. S. de Camargo, L. Canioni and T. Cardinal, *Crystals*, 2021, **11**, 148.
8 Y. M. Sgibnev, N. V. Nikonorov and A. I. Ignatiev, *J. Lumin.*, 2017, **188**, 172–179.
9 H. Fares, S. N. C. Santos, M. V. Santos, D. F. Franco, A. E. Souza, D. Manzani, C. R. Mendonça and M. Nalin, *RSC Adv.*, 2017, **7**, 55935–55944.
10 J. A. Jiménez, M. Sendova and C. Zhao, *J. Am. Ceram. Soc.*, 2015, **98**, 3087–3093.
11 J. Zhao, Z. Yang, C. Yu, J. Qiu and Z. Song, *Chem. Eng. J.*, 2018, **341**, 175–186.
12 R. Ma, J. Gao, Q. Xu, S. Cui, X. Qiao, J. Du and X. Fan, *J. Non-Cryst. Solids*, 2016, **432**, 348–353.
13 Z. Guo, S. Ye, T. Liu, S. Li and D. Wang, *J. Non-Cryst. Solids*, 2017, **458**, 80–85.
14 J. A. Jiménez and M. Sendova, *J. Alloys Compd.*, 2017, **691**, 44–50.
15 L. Bolundut, L. Pop, M. Bosca, G. Borodi, L. Olar, R. C. Suciu, P. Pascuta, E. Culea and R. Stefan, *Ceram. Int.*, 2017, **43**, 12232–12238.

16 F. Alassani, G. Galleani, G. Raffy, A. Del Guerzo, A. Royon, K. Bourhis, A. S. S. de Camargo, V. Jubera, L. Canioni, T. Cardinal and Y. Petit, *Opt. Mater. X*, 2022, **16**, 100205.
17 M. Ennouri, I. Jlassi and H. Elhouichet, *J. Non-Cryst. Solids*, 2021, **551**, 120397.
18 M. Sedano, G. Gorni, G. C. Mather, A. Durán, J. Fernández, R. Balda and M. J. Pascual, *J. Eur. Ceram. Soc.*, 2024, **44**, 2427–2436.
19 J. A. Jiménez, S. Lysenko, M. Sendova and C. Zhao, *Opt. Mater.*, 2015, **46**, 88–92.
20 W. Zheng, Z. Wang, W. Chen, M. Zhang, H. Li, G. Yang, Q. Xu, X. Qiao, D. Tan, J. Zhang, J. Qiu, G. Qian and X. Fan, *Nat. Commun.*, 2024, **15**, 8366.
21 A. Abou Khalil, J.-P. Bérubé, S. Danto, J.-C. Desmoulin, T. Cardinal, Y. Petit, R. Vallée and L. Canioni, *Sci. Rep.*, 2017, **7**, 11124.
22 F. Alassani, G. Raffy, M. Carpentier, J. Harb, V. Jubera, A. Del Guerzo, L. Canioni, T. Cardinal and Y. Petit, *ACS Appl. Mater. Interfaces*, 2024, **17**, 1770–1781.
23 F. Alassani, N. Ollier, G. Raffy, A. Fargues, A. Del Guerzo, L. Canioni, T. Cardinal and Y. Petit, *J. Phys. Chem. C*, 2024, **128**, 8296–8306.
24 M. de Oliveira, T. S. Gonçalves, C. Ferrari, C. J. Magon, P. S. Pizani, A. S. S. de Camargo and H. Eckert, *J. Phys. Chem. C*, 2017, **121**, 2968–2986.
25 G. Galleani, S. H. Santagneli, Y. Messaddeq, M. de Oliveira and H. Eckert, *Phys. Chem. Chem. Phys.*, 2017, **19**, 21612–21624.
26 D. S. Larionov, V. A. Bitanova, P. V. Evdokimov, A. V. Garshev, O. A. Shlyakhtin and V. I. Putlyaev, *Inorg. Mater. Appl. Res.*, 2024, **15**, 344–351.
27 Y. Petit, S. Danto, T. Guérineau, A. A. Khalil, A. Le Camus, E. Fargin, G. Duchateau, J. P. Bérubé, R. Vallée, Y. Messaddeq, T. Cardinal and L. Canioni, *Adv. Opt. Technol.*, 2018, **7**, 291–309.
28 A. Rajiv, M. Sudhakara Reddy, J. Uchil and N. Reddy, *J. Adv. Sci. Res.*, 2014, **5**, 32–39.
29 X. Shan, G. Tang, X. Chen, S. Peng, W. Liu, Q. Qian, D. Chen and Z. Yang, *J. Rare Earths*, 2016, **34**, 868–875.
30 J. A. Jiménez, *ACS Org. Inorg. Au*, 2024, **4**, 338–349.
31 R. Ma, J. Zhao, X. Chen, X. Qiao, X. Fan, J. Du and X. Zhang, *Phys. Chem. Chem. Phys.*, 2017, **19**, 22638–22645.
32 V. M. Khomenko, K. Langer and R. Wirth, *Phys. Chem. Miner.*, 2003, **30**, 98–107.
33 F. Ramos-Lara, C. A. Lira, M. O. Ramírez, M. Flores, R. Arroyo and U. Caldiño, *J. Phys.: Condens. Matter*, 2006, **18**, 7951.
34 I. Belharouak, E. Fargin, C. Parent, G. Le Flem, H. Aouad, M. Mesnaoui and M. Maazaz, *Solid State Sci.*, 1999, **1**, 287–300.
35 I. Belharouak, C. Parent, B. Tanguy, G. Le Flem and M. Couzi, *J. Non-Cryst. Solids*, 1999, **244**, 238–249.
36 N. Marquestaut, Y. Petit, A. Royon, P. Mounaix, T. Cardinal and L. Canioni, *Adv. Funct. Mater.*, 2014, **24**, 5824–5832.
37 Y. Shi, N. Zhao, Y. Chen, J. Liu, J. Li, Z. Hou and G. Zhou, *J. Non-Cryst. Solids*, 2023, **604**, 122139.
38 I. Belharouak, C. Parent, P. Gravereau, J. P. Chaminade, G. Le Flem and B. Moine, *J. Solid State Chem.*, 2000, **149**, 284–291.
39 J. J. Velázquez, V. K. Tikhomirov, L. F. Chibotaru, N. T. Cuong, A. S. Kuznetsov, V. D. Rodríguez, M. T. Nguyen and V. V. Moshchalkov, *Opt. Express*, 2012, **20**(12), 13582–13591.
40 S. Khan, S. K. Mohapatra, S. Chakraborty and K. Annapurna, *Opt. Mater.*, 2023, **143**, 114229.
41 J. C. Desmoulin, Y. Petit, L. Canioni, M. Dussauze, M. Lahaye, H. M. Gonzalez, E. Brasselet and T. Cardinal, *J. Appl. Phys.*, 2015, **118**, 213104.